RSC Advances

PAPER

View Article Online
View Journal | View Issue

Cite this: *RSC Adv.*, 2025, **15**, 34846

4-(4,6-Dimethoxy-1,3,5-triazin-2-yl)-4-methyl-morpholinium chloride-assisted amide crosslinking of carboxymethyl cellulose for high-performing films

Domenico Santandrea [ab] and Valentina Beghetto *[acd]

This study reports the first example of crosslinking of carboxymethyl cellulose (CMC) and aliphatic diamines (CMCA) using a condensation agent, (4-(4,6-dimethoxy-1,3,5-triazin-2-yl)-4-methyl-morpholinium chloride (DMTMM)), to prepare highly functional films for food packaging application. The novelty of this work lies in the combination of diamine crosslinking and DMTMM activation to produce films with enhanced barrier and mechanical properties. Products were analysed by mono-/bi-dimensional NMR to prove the amide linkage and by the modification degree (MoD) for diamine quantification. The physical–chemical characteristics of the CMCA films were further determined by DSC, TGA, SEM, and ATR-FTIR, and the moisture content (MC%), moisture uptake (MU%), water vapour permeability (WVP), oil absorption ratio (OAR), and tensile strength (TS) evidenced the key role of DMTMM in the formation of strong covalent bonds between the carboxylate groups of CMC and the diamine, influencing the properties of CMCA films. When a COONa/ethylenediamine/DMTMM molar ratio of 6/1/2 was employed, the best WVP ($2.63 \pm 0.24 \times 10^{-10}$ g m^{-1} s^{-1} Pa^{-1}), OAR ($7.4 \pm 0.5 \times 10^{-2}$%), and transparency were obtained, along with an exceptionally high UVC barrier and one of the highest TS values ever reported for CMC films (75.90 ± 2.90 MPa). Results clearly highlight that the presence of the diamine hydrophobic alkyl chain plays a key role in improving the physical–mechanical characteristics of CMCA, making it superior to the best-performing CMC films reported in the literature and as a sustainable alternative for food packaging applications.

Received 21st July 2025
Accepted 8th September 2025

DOI: 10.1039/d5ra05273d

rsc.li/rsc-advances

Introduction

The intensive use of non-biodegradable petroleum-based polymers is causing serious environmental problems. Due to their chemical and biochemical inertness, these materials tend to accumulate and break down into particles, generating micro- and nano-plastic contamination[1,2] and endangering the living beings on the Earth.[3–5] In this context, driven by the ambitions of the European Green Deal and the objectives of the 2030 agenda, it becomes increasingly important to seek eco-friendly and biodegradable materials that can reconcile economic growth with environmental sustainability. Biodegradable biopolymers, prepared from biomass waste,[6–9] represent a class of materials that can potentially reduce the impact of fossil-based products,[10–13] and their global production is expected to increase from 2.18 Mton in 2023 to approximately 7.43 Mton by 2028.[14]

Despite being extremely promising, polysaccharides exhibit some important drawbacks, such as poor dimensional stability, high hydrophilicity and lack of specific functional properties, that presently limit their potentiality.[15–18] Due to these problems, biopolymers are often chemically or physically modified to improve their properties.[7,19–25] For instance, carboxymethylcellulose (CMC), obtained by an alkali-catalysed reaction of cellulose with chloroacetic acid, is a very interesting and widely employed chemically modified biopolymer.[26–32] Nonetheless, due to the presence of a large number of carboxylic groups, CMC is water-soluble and requires to be further modified to improve its physical–mechanical characteristics.[33,34] Different strategies have been reported for this scope, among which grafting of CMC with an amine appears interesting to improve its hydrophobicity, yet this methodology has only been tested to promote the CMC solubility in organic solvents.[35–38] To the best of our knowledge, only very few works have studied the properties of films prepared by crosslinking of CMC;[25,39] in particular, Dacrory and coworkers reported the crosslinking of dialdehyde-CMC (DCMC) with succinic dihydrazide, showing

[a]*Dipartimento di Scienze Molecolari e Nanosistemi, Università Ca' Foscari Venezia, Via Torino 155, Venezia, 30172, Italy. E-mail: beghetto@unive.it; Tel: +39 412348928*
[b]*Dipartimento di Architettura e Disegno Industriale, Università della Campania "Luigi Vanvitelli", Via San Lorenzo-Abazia di San Lorenzo, Aversa, CE, 81031, Italy*
[c]*Crossing s.r.l., Viale della Repubblica 193/b, Treviso, 31100, Italy*
[d]*Consorzio Interuniversitario per le Reattività Chimiche e La Catalisi (CIRCC), Via C. Ulpiani 27, Bari, 70126, Italy*

that an increase in crosslinking density generates a rigid structure with a reduced water uptake capacity. Although their work clearly indicates that the formation of strong covalent crosslinking bonds could be a useful tool to improve the hydrophobicity of CMC films, the reagents they used by Dacrory were highly toxic, and thus, a more sustainable alternative should be identified.

Crosslinking represents an effective and well-known method used to modify biopolymer properties, such as hydrophobicity,[40–45] and it may be achieved by metal-ion complexation,[46] electrostatic interactions[47–49] or covalent bond formation.[50–54] The latter is often carried out in the presence of condensation agents added to promote the reaction.[55] 1-Ethyl-3-(3-dimethylaminopropyl)carbodiimide (EDC) and *N*-hydroxy succinimide (NHS) are widely employed in combination as condensation agents to promote amidation reactions.[56] Nevertheless, EDC and NHS decompose during the reaction, forming toxic compounds that need to be accurately removed from the product.[57] Alternatively, 4-(4,6-dimethoxy-1,3,5-triazin-2-yl)-4-methyl-morpholinium chloride (DMTMM) is a more sustainable and widely studied active condensation agent used for the synthesis of fine chemicals,[55,58–60] collagen or polysaccharides grafting,[61–63] and the crosslinking of various polymeric compounds.[52,64,65] In fact, DMTMM enables amidation reactions in water at room temperature, with the additional advantage that the by-products, 2,4-dimethoxy-6-hydroxy-1,3,5-triazine (DMTOH) and *N*-methyl morpholinium hydrochloride (NMM–HCl) (Scheme 1), formed during the reaction by DMTMM decomposition are non-toxic, water-soluble and easily removed by washing or dialysis.[66] Furthermore, the superior efficiency of DMTMM against EDC/NHS for cellulose amidation has been proven by Kumar and coworkers.[67] Additionally, DMTMM is a "zero-length" activating condensation agent and therefore is not incorporated in the product. This characteristic is of particular importance for food packaging applications as DMTMM does not remain in the final product (confirmed by cytotoxicity tests reported in the literature).[52]

Although many different grafting and crosslinking reactions of CMC have been reported in the literature in the presence of EDC/NHS,[38] epichlorohydrin,[68] aldehyde-based reagents,[18] urea derivatives,[26] and carboxylic acids,[27,69–71] to the best of our knowledge, the crosslinking of CMC in the presence of diamines and DMTMM has never been reported.

Only one example exists of the self-crosslinking of CMC performed in the presence of DMTMM, promoting the condensation reaction between the carboxylic and hydroxyl functional groups present in CMC (Scheme 1) and producing films with highly improved physical–mechanical characteristics and hydrophobicity compared to existing materials.[51] Within this panorama, the hypothesis of this work is that the crosslinking of CMC with aliphatic diamines (CMCA) promoted by 4-(4,6-dimethoxy-1,3,5-triazin-2-yl)-4-methyl-morpholinium chloride (DMTMM) will generate CMCA films with good water vapour barrier properties and superior physical–mechanical characteristics, making them adequate for food packaging applications. In fact, DMTMM can efficiently promote the condensation of the carboxylate functional groups of CMC and the diamines, generating a compact polymeric network and improving the physical–mechanical performances and UV barrier properties of the films. Meanwhile, the hydrophobic

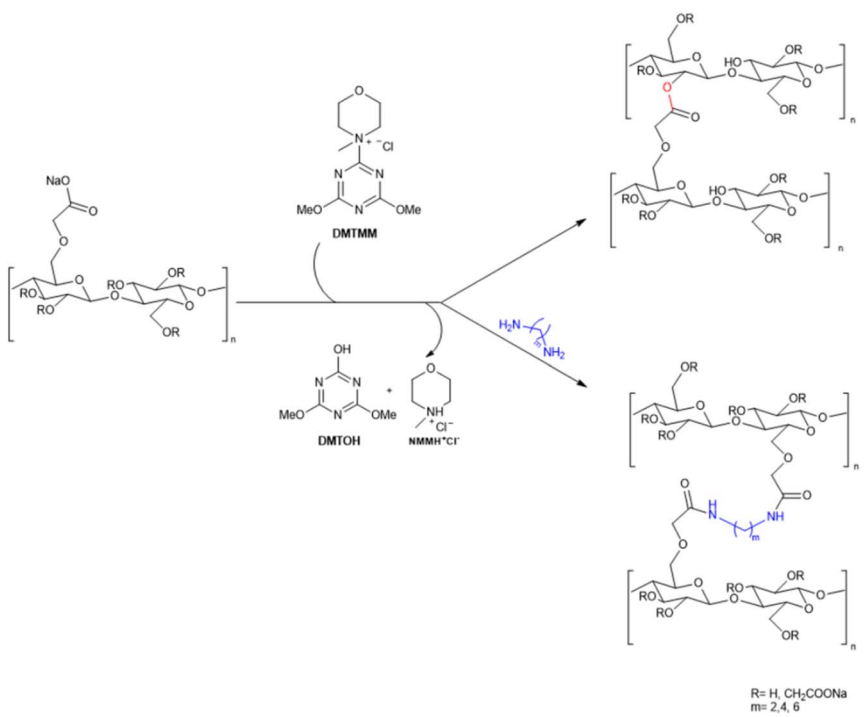

Scheme 1 Proposed mechanism for CMC crosslinking promoted by DMTMM by self-condensation (above) and in the presence of a diamine (below).

alkyl chain of the diamines reduces water diffusion and consequently improves the water vapour barrier properties.

Thus, the modification degree and physical–mechanical characteristics of films prepared with different aliphatic diamines (with increasing alkyl chain length) at variable COONa/diamine/DMTMM molar ratios were tested. All films obtained by casting technology were characterised by NMR, elemental analysis, UV-vis, DSC, TGA, SEM, ATR-FTIR, and mechanical tests, and their transparency, colour properties, moisture content, moisture uptake, water vapor permeability, and oil resistance ability were evaluated. The obtained data were compared with those for non-crosslinked CMC films. Finally, biofragmentation tests were carried out to evaluate the end-of-life of the films. The results demonstrate that the synergistic use of DMTMM and an aliphatic diamine allows the achievement of CMCA films having some of the best physical–mechanical characteristics reported in the literature for CMC-based films, making them highly promising candidates for food packaging applications.

Experimental section

Materials

CMC (with a carboxylation degree of DS = 0.7 and an average molecular weight of 90 000 Da), ethylenediamine (EDA), 1,4-diaminobutane (DAB), 1,6-diaminohexane (DAH), and DMTMM were purchased from Sigma-Aldrich Co. (St. Louis, MO) and used as received.

Methods

Crosslinking of CMC in the presence of a diamine and DMTMM and film casting. CMC was crosslinked with COONa/diamine/DMTMM in different molar ratios (see Table 1). For example, film F1 was prepared as follows: 0.5 g of CMC (1.60 mmol of COONa groups) was solubilized in 10 mL of distilled water. Meanwhile, a solution containing 10 mL of water and 31.6 mg of DAH (0.27 mmol, COONa/DAH 6/1 mol/mol) was prepared, neutralized with 0.1 M HCl to achieve pH 7, and 150 mg of DMTMM (0.54 mmol, DAH/DMTMM = 1/2 mol/mol) was added.

The diamine/DMTMM solution was added to the CMC solution, and the whole system was left under stirring for 20 h at room temperature (rt). The viscous solution obtained was dialyzed using a dialysis tube (1000 Da molecular weight cut off) with a 0.1 M NaCl water solution for 72 h and with distilled water for 48 h, changing the water daily. The resulting clear solution was transferred into a polystyrene Petri dish (9 cm diameter) and oven dried at 35 °C for 48 h. All films were prepared following this procedure with the molar ratios reported in Table 1, followed by casting. Control CMC films (F0) were prepared by dissolving 0.5 g of CMC in 20 mL of water under vigorously stirring at room temperature until total dissolution was achieved (30 min). The resulting solution was cast as film F1. The identification codes of all films prepared in this work are reported in Table 1.

Detailed product yields, expressed as the ratio between the mass of the crosslinked film and the sum of the mass of the starting CMC and diamine,[76] are reported in Tables 1 and S1 in the SI section.

Characterization of the films

^{1}H, ^{13}C and bidimensional NMR characterisation and elemental analysis. The ^{1}H, ^{13}C, COSY and HSQC NMR spectra were recorded using a Bruker Advance 300 spectrometer (Milano, Italy) operating at 300.13 MHz for the proton spectrum and 75.4 MHz for the carbon spectrum, with chemical shifts reported on a δ-scale (ppm). Each sample (50 mg) was dissolved in deuterated water (0.6 mL). 64 scans for ^{1}H, 48k scans for ^{13}C, 64 scans for COSY and 124 scans for HSQC were collected. HMBC (Heteronuclear Multiple Bond Correlation) NMR experiments were performed on a 600 MHz high-resolution spectrometer to identify long-range heteronuclear correlations.

The degree of modification (MoD_{NMR}) was determined from the ^{1}H NMR spectra of CMC and CMCA by treating 50 mg of the sample with 0.5 mL of deuterated water and 0.5 mL of deuterium chloride at 95 °C for 1 h. 64 scans were collected for each

Table 1 MoD_{th}, MoD_{NMR} and elemental analysis of the CMCA films

Sample	DA[a]	COONa/DA/DMTMM[b] (mol/mol/mol)	CMC/DMTMM (wt/wt%)	MoD_{th}[c] (%)	MoD_{NMR}[d] (%)	MoD_{NMR}/MoD_{th}	C[e] (%)	H[f] (%)	N[g] (%)	Yield[h] (%)
F1	DAH	6/1/2	30	24	7.00	0.29	41.58	5.3	0.52	95
F1′	DAH	6/1/0	—	—	—		—		—	
F2	DAH	3/1/2	60	47	9.25	0.19	40.58	5.1	0.60	91
F3	DAH	6/0.5/1	15	12	3.75	0.31	43.32	5.4	0.25	97
F4	DAB	6/1/2	30	24	9.00	0.38	47.24	5.6	0.67	97
F5	DAB	6/0.5/1	15	12	4.75	0.24	46.50	5.5	0.35	99
F6	EDA	6/1/2	30	24	9.75	0.40	44.81	5.4	0.71	98
F7	EDA	6/0.5/1	15	12	4.75	0.39	43.61	5.4	0.32	98

[a] DA: diamine. [b] COONa/DA/DMTMM: molar ratio calculated based on the mmol of COONa present in 0.5 g of CMC (1.60 mmol). [c] MoD_{th}: theoretical modification degree: $(NH_{2i}/AGU_{tot}) \times 100$, where the AGU_{tot} in 0.5 g of CMC is 2.29 mmol and NH_{2i} is the initial mmol of the amine group. [d] MoD_{NMR}: see eqn (1) and (2) in the Experimental section. [e] C%: carbon content obtained by elemental analysis. [f] H%: hydrogen content by elemental analysis. [g] N%: nitrogen content by elemental analysis. [h] Product yield, expressed as the grams of product recovered after dialysis, relative to the total grams of starting CMC and diamine used.

sample. The degree of modification was calculated according to eqn (1) for all films except for F6 and F7 (see below):

$$\mathrm{MoD_{NMR}}\ (\%) = \frac{I_{\mathrm{int}}/4}{I_{4.5-5.5\,\mathrm{ppm}}} \times 100 \quad (1)$$

where I_{int} is the area of the signal of the most internal methylene group in the diamine and $I_{4.5\text{–}5.5\ \mathrm{ppm}}$ is the area of the anomeric proton (see Fig. S15–S19). Since the methylene groups of EDA overlap with the anhydroglycosidic unit (AGU) signals between 3.0 and 4.0 ppm, the $\mathrm{MoD_{NMR}}$ for films F6 and F7 were calculated according to eqn (2):

$$\mathrm{MoD_{NMR}}\ (\%) = \frac{\frac{I_{(3.0-4.0\,\mathrm{ppm})} - 6}{4}}{I_{4.5-5.5\,\mathrm{ppm}}} \times 100 \quad (2)$$

where $I_{3.0\text{–}4.0\ \mathrm{ppm}} - 6$ represents the area of the protons in α position to the nitrogen of the covalently linked diamine and $I_{4.5\text{–}5.5}$ ppm represents the area of the proton in the C1 anomeric position (Fig. S20 and S21).

Elemental analyses (CHN) were performed using the Unicube Organic Elemental Analyser (Unicube, Lomazzo (CO)), and data reported are the mean value of three replicates.

UV-vis analysis and transparency measurements

The UV-vis spectroscopy analysis of all CMC films prepared was carried out using an Agilent Cary 100 UV/vis spectrophotometer (Milano, Italy). The films were placed into the spectrophotometer test cell, and air was used as a reference. The optical absorbance/transmittance of the films was measured in the wavelength range of 200–800 nm with a scan rate of 600 nm $\mathrm{min^{-1}}$. Transparency tests were carried out on the CMC films by measuring the absorbance at 600 nm and thereafter performing calculations according to eqn (3):

$$\mathrm{Transparency} = (\log T_{600})/t \quad (3)$$

where T_{600} is the value of transmittance at 600 nm and t is the film thickness (mm). All measurements were performed in triplicate.

Colour of the films

The colour of all the CMC films was evaluated using a spectrocolorimeter (Konica Minolta sensing Inc., CM 2600d, Osaka, Japan) equipped with a D65 standard illuminant, and the specular component excluded mode was used. The results were expressed as L^* (lightness), a^* (redness) and b^* (yellowness), using a white plate as the standard ($L^* = 91.76$, $a^* = 4.12$, $b^* = -10.9$). All measurements were performed in triplicate on three random locations for each film. The total colour difference (ΔE), yellow index (YI), and white index (WI) were calculated according to eqn (4)–(6):

$$\Delta E = \sqrt{\left(L_s^* - L^*\right)^2 + \left(a_s^* - a^*\right)^2 + \left(b_s^* - b^*\right)^2} \quad (4)$$

$$\mathrm{YI} = \frac{146.86 \times b^*}{L^*} \quad (5)$$

$$\mathrm{WI} = 100 - \sqrt{(100 - L^*)^2 + a^{*2} + b^{*2}} \quad (6)$$

Film thickness

Film thickness was measured with a Lhomargy micrometer (Saint-Baldoph, France) having a sensitivity of ± 0.001 mm. The Measurements were made at different points (at least five) on the same film (at 25 ± 2 °C, RH = 55%), and the average values were calculated.

Moisture uptake (MU%)

All CMC films (20 mm × 20 mm) were first conditioned in a desiccator containing anhydrous $CaSO_4$ at 0% relative humidity (RH) until constant weight was achieved (W_o, 48 h at 25 ± 2 °C), followed by further conditioned with a saturated solution of K_2SO_4 (RH = 97%) until constant weight was registered (W, 48 h at 25 ± 2 °C). All measurements were performed in triplicate. The moisture uptake (MU%) value of the samples was calculated according to eqn (7):

$$\mathrm{MU}\ (\%) = [(W - W_o) \times 100]/W_o \quad (7)$$

Moisture content (MC%)

The CMC film samples (20 mm × 20 mm) were first conditioned using $CaNO_3$ (RH = 55%) for 48 h at 25 ± 2 °C, weighed (W_o) and then dried in an oven at 105 °C until a constant weight was obtained (W_f). All measurements were performed in triplicate. The moisture content (MC%) of the samples was calculated according to eqn (8):

$$\mathrm{MC}\ (\%) = [(W_o - W_f) \times 100]/W_o \quad (8)$$

Water vapor permeability (WVP)

WVP (g $\mathrm{m^{-1}\ s^{-1}\ Pa^{-1}}$, eqn 9) tests were carried out according to the ASTM standard method.[79] Cups with an average diameter of 3.5 cm and a volume of 70 mL were used to determine the WVP of the films. Each cup was covered with a film and sealed using paraffin. Cups containing anhydrous $CaCl_2$ (RH = 0%) were placed in a conditioned room with RH = 55%. Air circulated through the chamber in order to maintain uniform conditions during measurements. The cups were weighed every 1 h for the first 10 h and finally after 25 h. The water vapor transmission rate (WVTR) was calculated from the slope of the increase in weight over time (g $\mathrm{s^{-1}}$) divided by the exposed film area ($\mathrm{m^2}$) eqn (9) (g $\mathrm{m^{-2}\ s^{-2}}$):

$$\mathrm{WVP} = (\mathrm{WVTR} \times t)/[P(R_1 - R_2)] \quad (9)$$

where t is the film thickness (m), P is the saturation vapor pressure (Pa) at 25.0 ± 2 °C, R_1 is the RH in the room (0.55) and R_2 the RH in the cup (0). Under these conditions, the driving force $[P(R_1 - R_2)]$ is 1753.55 Pa, expressed as water-vapor partial pressure.[80] All measurements were performed in triplicate.

Oil resistance ability of films (OAR, %)

The oil resistance of the films was tested according to a literature protocol.[81] Filter paper (6 cm in diameter) was oven-dried at 50 °C until a constant weight was reached. Film samples (4 cm in diameter) were fixed with parafilm on the top of a glass test tube containing 5 mL of sunflower oil and were placed on the filter paper upside down for 48 h. Then, the filter paper was weighed, and the oil absorption rate (OAR) was calculated according to eqn (10):

$$\text{OAR } (\%) = (m - m_o)/m_o \times 100 \quad (10)$$

where m is the weight of filter paper after 48 h and m_o is the weight of dried filter paper.

Differential scanning calorimetry (DSC) and thermal gravimetric analysis (TGA)

DSC analysis of all films was performed on a DSC 3 (Mettler Toledo, USA). The instrument was calibrated using indium as the standard. CMC samples (about 5.0 mg) were weighed into an aluminium-oxidized melting pot, sealed and heated from 30 °C to 250 °C at a heating rate of 10 °C min^{-1}. A sealed melting pot filled with Al_2O_3 (about 7.0 mg) was used as the reference. TGA of all films (about 10 mg) was carried out on a STA PT-1000 (Linseis, Germany) from 30 °C to 500 °C at the rate of 10 °C min^{-1} under a nitrogen flow of 50 mL min^{-1}.

SEM analysis

The morphology and the microstructure of the film surface were observed by scanning electron microscopy with an ESEM Philips XL30 TMP Microanalysis XRF-EDS. SEM analysis was carried out on the surface of the films, which were gold-coated applying a K450X sputter coater (Emitech, England) under 10^{-1} Pa vacuum. The images of the sputtered-coated film samples were captured at an accelerating beam voltage of 25 kV.

Mechanical properties

The tensile strength (TS) and elongation at break (EB) of the films were determined at 25 ± 1 °C preconditioned to RH = 55% for 48 h using a tensile tester RSA3 (TA Instruments, USA), according to the ASTM standard method D882-91. Film specimens (5.0 × 1.5 cm) were mounted between the grips of the machine. The initial grip separation and crosshead speed were set to 30 mm and 5 mm min^{-1}, respectively. All measurements were performed in triplicate.

ATR-Fourier transform infrared spectroscopy (ATR-FTIR)

ATR-FTIR spectra of all CMC films were recorded on a FT-IR PerkinElmer 1720X spectrometer (Milano, Italy) in attenuated total reflectance (ATR) mode. The ATR-FTIR spectra were collected with a resolution of 2 cm^{-1} in the range of 4000–650 cm^{-1}. Thus, 16 scans were acquired within this interval with at least two duplicates for each sample.

Biofragmentation tests

Biofragmentation of films F0, F1, and F3–F7 was carried out according to the literature, with slight modifications.[72] Soil was poured into plastic trays (7 × 13 × 4 cm), and samples of each film (2 cm × 2 cm) were weighed and then buried in the soil to a depth of 2 cm at 25 °C and 50% RH. The soil was sprayed with water once a day. At different times (third and seventh day), samples were carefully taken out and photographed. Biofragmentation was assessed by visual testing since it was impossible to wash and weigh the films due to their advanced state of degradation. The pH of the soil was determined with an XS pH 8 Standard Table pH Meter, after dispersing 1 part by weight of soil in 20 parts of water, following ASTM G160-12. The soil showed a pH of 7.17.

Statistical analysis

Statistical analysis results of multiple samples tested are reported. Average values ± standard deviation were calculated using one-way and two-way analysis of variance (ANOVA) by means of the OriginPro 2019 software. Differences among the mean values were processed by Tukey's multiple range test. Significance was defined at $p < 0.05$. All experiments were performed in triplicate.

Results and discussion

Crosslinking amidation reaction of CMC in the presence of DMTMM and film casting

The amidation reaction between CMC and different diamides (DAH, DAB and EDA) was tested in the presence of DMTMM as the activating crosslinking agent (Scheme 2). It is well known from the literature that the triazine ring of DMTMM can react with the carboxyl groups of a polymer, thereby generating an active ester and promoting the reaction with a nucleophile, in this case a diamine.[57,58] In order to assess the optimal reaction conditions and general reaction scope, the efficiency of DMTMM (see Table 1) was tested with varying the stoichiometric ratios of the reagents and the length of the alkyl chain of the diamines.

In Table 1, the CMC/DMTMM wt/wt% ratios are also given, as it is normal practice in the literature to use the crosslinking agent in wt% rather than molar ratios, allowing for a better comparison with previous works. Additionally, the molar ratios between reagents were used in order to assess the influence of the stoichiometric ratio between COONa/diamine/DMTMM on the physical–mechanical characteristics of the films derived. In particular, experiments were carried out with different COONa/diamine/DMTMM molar ratios, based on the mmol of the COONa functional groups present in 0.5 g of CMC (1.60 mmol) (see Table 1). The reaction was carried out at room temperature in water. The pH was carefully kept at pH 7 by neutralizing the amino groups with a hydrochloric acid solution, since the efficiency and stability of DMTMM strongly depend on the pH of the reaction medium and good performance is generally obtained in the range of 5 < pH < 9.[62,64,73,74] After 20 h, the solution was dialysed to remove the by-products of the condensing agent

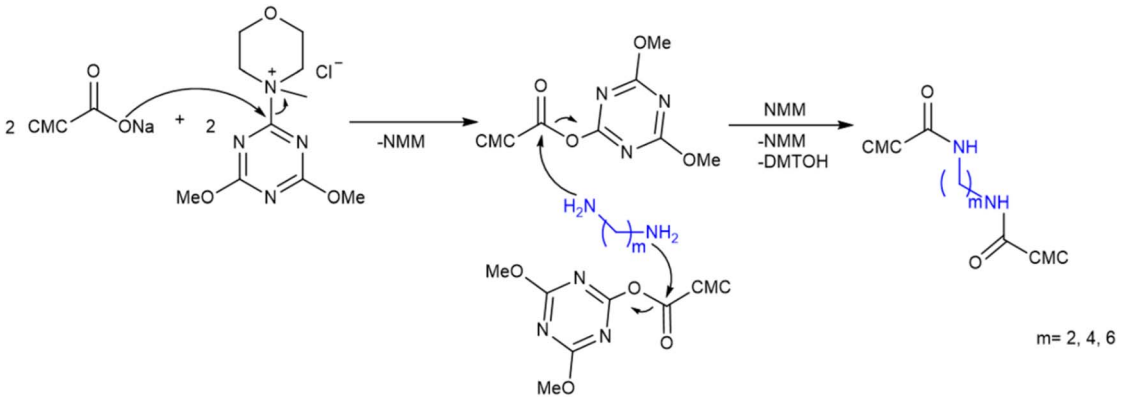

Scheme 2 Proposed reaction mechanism of CMC and diamine crosslinking promoted by DMTMM.

(DMTOH and NMMHCl) and unreacted diamine, and films were prepared by casting technology. The chosen cut-off of the dialysis tube (1000 Da) allowed the purification of the crosslinked CMC from low-molecular-weight unreacted species and DMTMM by-products (MW_{DMTMM} = 276.72 Da; MW_{NMMHCl} = 137.61 Da; MW_{DMTOH} = 157.13 Da; MW_{EDA} = 60.10 Da; MW_{DAB} = 88.15 Da; MW_{DAH} = 116.21 Da) and the quantitative recovery of the product in high yields (between 91% and 99%). As far as the yield of CMCA after dialysis and casting is concerned, different calculations have been reported in the literature. For example, Šimkovic and coworkers calculated the yield based on the final weight of the film divided by the weight of CMC initially used, disregarding the weight of the crosslinker, and yields as high as 120% were reported.[25] Alternatively, Kono measured the yield as the ratio between the final weight of the film obtained by casting and the sum of the weight of CMC and crosslinker initially introduced in the reaction mixture, reporting yields between 85% and 91%.[75] This second approach was preferred in this work.

Characterisation of CMC films by NMR and elemental analysis

In order to verify the efficiency of the crosslinking agent, preliminary experiments were carried out in the presence of DAH, selected as the model reactant, with a COONa/diamine/DMTMM molar ratio of 6/1/2 or without DMTMM, and the data were compared with those for control sample F0. After 20 h, both solutions were dialysed with a 0.1 M NaCl water solution to remove DMTOH, NMMHCl and unreacted amine, followed by casting to prepare films F1, F1′ and F0. A comparison of the ^{1}H and COSY NMR spectra of F0, F1 and F1′ (Fig. S1 and 1a) confirms that the presence of DMTMM is crucial in determining strong bonds, as all the diamine is removed if no condensing agent is employed (F1′, Fig. S1). In fact, the COSY spectra of F1 further revealed the presence of a new signals at 3.26/1.54 and 2.99/1.67 ppm, due to the interaction between CMC and the diamine (Fig. 1a and S4). Additional valuable information on the chemical nature of the crosslinking was obtained by comparing the HMBC spectra of F0 and F1 (Fig. S11 and 1b). The presence of three cross-peaks in the carbonyl region (4.00–4.28/178.05 ppm) of the HMBC spectra of F0 (Fig. S11) and F1 is in accordance with the literature, due to the presence of carboxymethyl moieties in positions 2, 3 and 6 of the AGU unit.[76,77] Interestingly, the HMBC spectrum of the CMC crosslinked with DAH (F1, Fig. 1b) showed a shift of the signals of the carbonyl moiety from 4.00–4.28/178.05 ppm to slightly lower ppm, consistent with changes in the chemical environment of the carboxymethyl moieties due to carbonyl group conversion. In addition, a correlation was observed between the terminal methylene of the diamine and the carbonyl group at 3.25/160–170 ppm (F1, Fig. 1b), consistent with the newly formed amide linkages (CH_2–NH–C=O).[76]

The cross-peaks at 1.40–1.67/25–40 ppm in F1 correspond to the methylene units of the DAH chain. Notably, in the HSQC spectra, the signal of the terminal methylene of the diamine chain was only moderately shifted from 2.63/42.76 ppm in the free diamine to 2.99/42.17 ppm (Fig. S8 and S14). In addition, no correlation was detected between the protons at 2.99 ppm and the carbonyl carbon in the HMBC, further supporting the occurrence of simple ionic rather than covalent interactions in the crosslinking of CMC. A pure ionic–ionic crosslinking can be excluded since all unbound amines were removed by dialysis (see Fig. S1).

Analogous considerations are valid for the CMC films crosslinked with DAB and EDA, and all spectra are reported in SI (^{1}H, ^{13}C, COSY, HSQC and HMBC). In particular, in the case of EDA, the diamine signals appear at higher ppm regions, overlapping with the AGU region in the monodimensional ^{1}H NMR spectra (Fig. S2). This makes the two-dimensional spectra even more essential for identifying the diamine signals and confirming the presence of covalent amide linkages through the observation of characteristic cross-peaks in the HMBC spectrum (Fig. S13). ^{1}H NMR studies were further employed to determine the modification degree of CMCA films, as described in ^{1}H, ^{13}C and bidimensional NMR characterisation and elemental analysis. To improve the resolution of the monodimensional ^{1}H NMR spectrum, a protocol reported by Ho & Klosiewicz was adopted, involving dissolving films in D_2O/DCl (see SI, Fig. S15–S21).[77] In D_2O/DCl, the anomeric protons of the AGU ring are present between 4.9 and 5.8 ppm, methylene

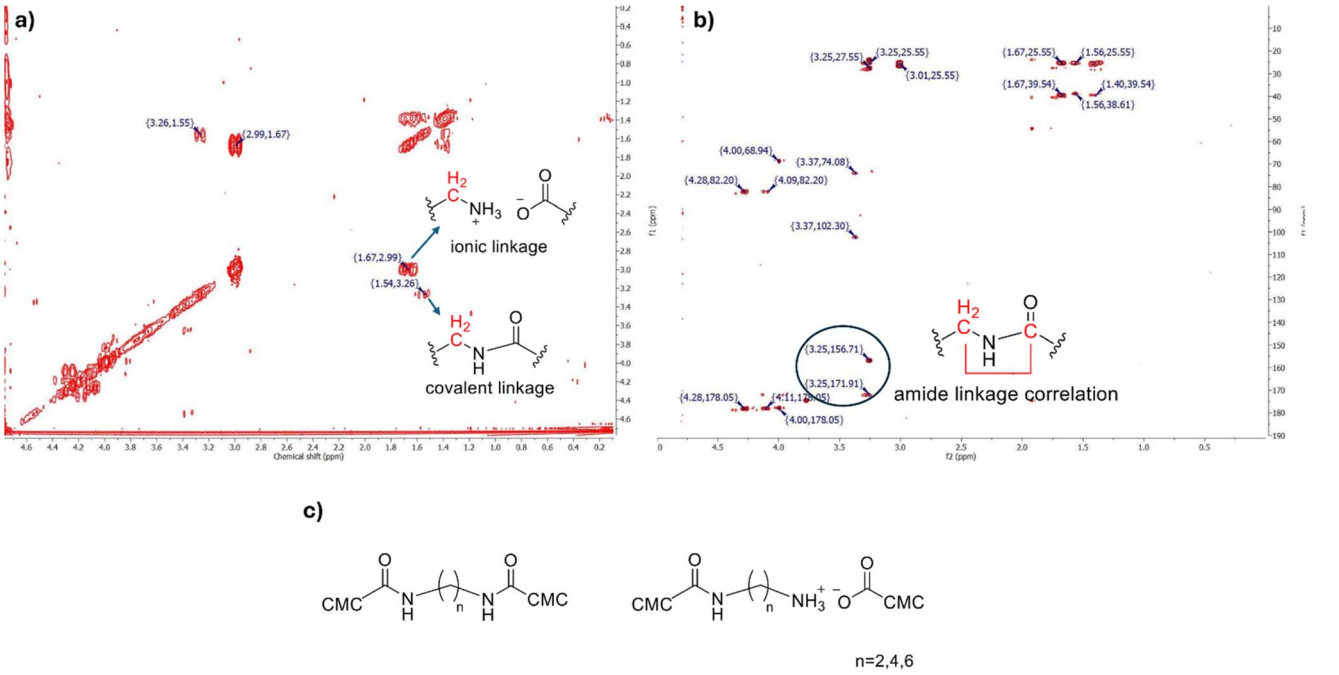

Fig. 1 (a) COSY NMR of F1, (b) HMBC of F1, and (c) schematic of the crosslinking.

protons of CH_2COONa functional groups are visible between 4.0 ppm and 4.5 ppm, while the non-anomeric protons can be found between 3.1 ppm and 3.8 ppm.[77–79] Finally, the signals around 3.0 ppm correspond to the methylene groups in the α position relative to the nitrogen, and those between 1.2 ppm and 1.8 ppm correspond to the alkyl chain of the diamine.

To determine the modification degree in the reaction between diamines and CMC, MoD_{th} and MoD_{NMR} (theoretical and NMR-measured) were calculated following a similar procedure reported in the literature.[80] MoD_{th} was calculated as the ratio between the mmol of NH_2 initially added (NH_{2i}) and the total mmol of anhydroglucose units (AGU_{tot}) present in 0.5 g of CMC (2.29 mmol), representing the theoretical maximum degree of modification allowed. The MoD_{NMR} was determined from the ^{1}H NMR spectra of CMC according to eqn (1) and (2) (see the Materials and Method section and ref. 80), corresponding to the modification degree actually obtained. The resulting MoD values are reported in Table 1 and range from 3.75 to 9.25, depending on the type of diamine used and the stoichiometric ratios applied. In particular, experiments carried out with double the mmol of DAH and DMTMM gave no significant improvement in the crosslinking of CMC (COONa/DAH/DMTMM 3/1/2, film F2, Table 1 and Fig. S16). This is probably because, as reported in the literature,[81,82] the efficiency of DMTMM tends to reach a plateau due to steric hindrance phenomena, especially when it is employed to promote polymer crosslinking. Thus, quantities of DMTMM above 30 wt/wt% by weight of CMC are unnecessary and were therefore not further investigated. On the contrary, the MoD_{NMR}/MoD_{th} ratio was almost equivalent to that for F1 when half the mmol of DAH was used (see F1, F3, Table 1 and Fig. S17). Notably, the MoD_{NMR} tends to increase when shorter diamines are used, probably because steric hindrance effects are reduced, thereby enhancing the reaction efficiency. The C (%), H (%), and N (%) values for all samples were determined by elemental analysis and are reported in Tables 1 and S2. To verify the consistency with the NMR data, the nitrogen percentage (% N) was also calculated based on the NMR results by estimating the mmol of reacted diamine. The calculated % N was found to be very similar to the value obtained from elemental analysis, confirming the reliability of both techniques when used together. An example of the calculation for sample F1 is provided in SI, and the data for all samples are reported in Table S2. Further characterisation was carried out on films with the highest MoD_{NMR}/MoD_{th} ratio (F1, F3, F4, F5, and F6) and the results compared with that for control sample F0.

Colour, transparency, UV-vis analysis and thickness

Colour parameters, transparency and UV-vis spectra were measured to assess information on the optical properties of the films, which are particularly important for the potential application of CMCA films for food packaging. A list of all colorimetric parameters is reported in Table 2. No significant differences in lightness (L^*), yellowness (a^*) and whiteness (b^*) were observed between control sample F0 and crosslinked films F1 and F3–F7, demonstrating that crosslinking does not significantly alter the good optical properties of pure CMC films, which are not distinguishable by the naked eye. Both the colour difference (ΔE) and yellow index (YI) are slightly lower for F3, F5, and F7 films compared to F1, F4, and F6 films, while no significant differences were observed for the white index (WI) (see Table 2).

The transparency values of films F0, F1, and F3–F7 (see Table 2 and Fig. 2a) showed noticeable differences; in particular, films

Table 2 Hunter colour values (L^*, a^* and b^*), total colour difference (ΔE), yellowness index (YI), whiteness index (WI), transparency (T_r) and thickness of films F0, F1, and F3–F7[a]

Film	L^*	a^*	b^*	ΔE	YI	WI	T_r	t (μm)
F0	87.58 ± 0.14	3.67 ± 0.01	−9.46 ± 0.01	4.45 ± 0.01	−15.86 ± 0.02	83.96 ± 0.85	33.31 ± 0.07	59 ± 1
F1	88.29 ± 0.18	3.81 ± 0.01	−10.08 ± 0.01	3.58 ± 0.01	−16.77 ± 0.03	84.09 ± 0.74	39.28 ± 0.09	50 ± 4
F3	88.94 ± 0.20	3.88 ± 0.02	−10.15 ± 0.01	2.93 ± 0.02	−16.76 ± 0.05	84.49 ± 0.66	41.96 ± 0.24	47 ± 2
F4	87.56 ± 0.15	3.49 ± 0.01	−8.80 ± 0.01	4.75 ± 0.01	−14.76 ± 0.04	84.37 ± 0.35	27.30 ± 0.09	62 ± 1
F5	88.15 ± 0.11	3.81 ± 0.01	−9.89 ± 0.01	3.77 ± 0.01	−16.48 ± 0.02	84.10 ± 0.19	36.40 ± 0.17	54 ± 2
F6	87.85 ± 0.07	3.47 ± 0.01	−8.71 ± 0.01	4.54 ± 0.01	−14.56 ± 0.02	84.65 ± 0.20	30.08 ± 0.38	66 ± 3
F7	88.43 ± 0.01	3.80 ± 0.01	−9.91 ± 0.01	3.49 ± 0.01	−16.46 ± 0.04	84.30 ± 0.23	39.03 ± 0.26	50 ± 3

[a] T_r: transparency measured at 600 nm; t: film thickness (μm). Values given are mean ± standard deviation.

F3, F5, and F7 exhibited higher transparency compared to the control sample F0 (see Table 2 and Fig. 2a).[83] On the contrary, when higher quantities of DMTMM were employed (CMC/DMTMM 30 wt/wt%), the transparency at 600 nm decreased, analogous to the data reported for DCMD–gelatine films.[84]

The UV-vis spectra of films F0, F1, and F3–F7 were registered in absorption and transmittance mode between 200 nm and 800 nm (Fig. 2b and c), and the shielding performance was measured at three different wavelengths (250 nm, 300 nm, 350 nm), representative of UVC, UVB, UVA[85] (Fig. 2d), respectively. These data are particularly relevant to define the specific application, since such radiations generate undesired photochemical processes (cleavage of covalent bonds, generation of free radicals), responsible, for example, for the photodegradation of lipids in food.[84,86,87] While the shielding effects of F1, F3–F7 and F0 against UVB and UVA are similar, a significant decrease in UVC transmittance is observed for the sample with the highest degree of modification (*i.e.* F6), which reduced the transmittance at 250 cm^{-1} to 93% compared to the results for F0. In agreement with the literature, the improvement in the UVC shielding properties is a consequence of the crosslinking of the polymer matrix. This improvement increases surface density,[51,52,88–90] an important characteristic for food packaging. For completeness, optical images of films F0, F1, and F3–F7 are reported in Fig. 2e. Regarding sample thickness, the moderate differences observed (Table 2) are mainly attributable to the mass loss (about 7–18%) occurring during purification by dialysis, rather than to differences in swelling related to the crosslinking degree, as previously suggested in the literature.[91]

Determination of moisture uptake, moisture content, water vapor and oil permeability

Moisture content percent (MC%), moisture uptake percent (MU%), and water vapour permeability (WVP) were measured,

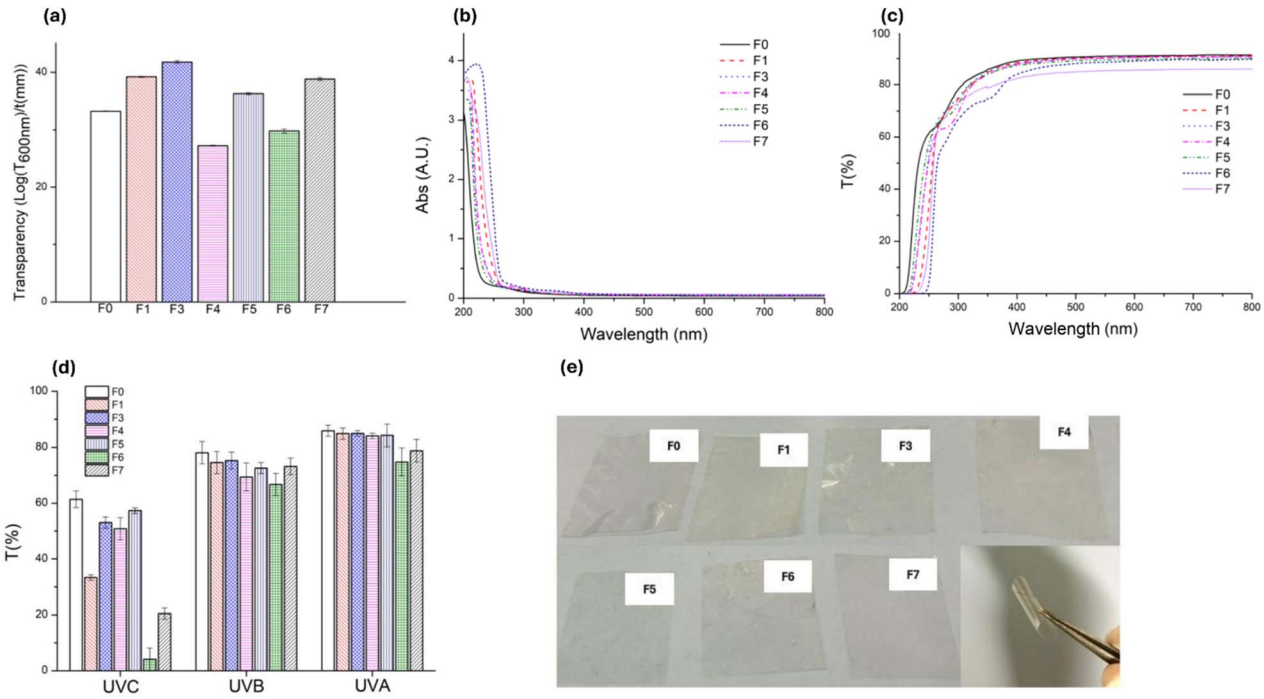

Fig. 2 (a) Transparency, (b) absorbance spectra, (c) transmittance spectra, (d) UVC, UVB, and UVA transmittance and (e) optical images of samples F0, F1, F3–F7.

and the data for F1 and F3–F7 and the control sample F0 are reported in Table 3. These characteristics are also very important for the packaging industry, helping preserve food from the surrounding environment.[92] For all CMCA films, the MC%, MU% and WVP values seem to be more influenced by the type of diamine used and less by the amount of DMTMM used. Interestingly, a reduction of up to 16% was registered for the MC% values of F1, F3, F4 and F5 crosslinked with DAH or DAB and slightly less for the films prepared with EDA (10% for F6 and F7).

Analogously, the MU% values decrease from 98.4 ± 3.5 for F0 to 69.6 ± 2.1 for F1 (<27%), while only moderate changes were observed when the amount of DMTMM employed was varied (see Table 3). Regarding WVP values, films F1 and F3–F7 exhibited similar behavior, with a significant reduction in WVP of up to 55% for F4, F6, and F7 compared to the control sample F0, highlighting the positive effect of crosslinking on water vapor permeability. Since MU%, MC% and WVP are very important characteristics for food packaging applications, careful comparison with literature data was carried out to highlight the performances of the films obtained by the crosslinking amidation of CMC.

Considering the CMCA films (Table 3) with respect to the CMC films self-crosslinked with DMTMM (CMC/DMTMM)[51], an overall decrease in MC%, MU% and WVP was registered (21%, 13% and 38%, respectively), showing that the use of diamines reduces the water affinity of CMCA films. This is probably a consequence of both the superior efficiency of DMTMM towards the formation of amide compared to ester bonds[93] and the high hydrophobicity of the polymer matrix due to the presence of the apolar methylene groups of the diamines. Further comparison of the MC%, MU%, WVP values and other general physical–mechanical characteristics of the CMC films is rather difficult since, although many works have been published on the crosslinking of CMC, the substitution degrees may differ and the molecular weight is often not reported.[94–96]

Nonetheless, on comparing the CMCA films with other CMC based films, it emerges that the MC%, MU% and WVP values of F1 and F3–F7 are comparable to or higher than other literature data. For example, compared to the CMC films prepared in the presence of fatty acid esters (MC% of 35.08 ± 0.16, WVP of 2.29 ± 0.30 × 10^{-9} g m^{-1} s^{-1} Pa^{-1}) (Mukherjee *et al.*, 2024),[96] the MC% values of the CMCA films are similar, while the WVP values are distinctively higher. Additional comparisons are given only for the WVP, since the MC% and MU% were not easily determined.

Shahbazi and coworkers studied the preparation of CMC and polyvinyl pyrrolidone films crosslinked with 15 wt% glutaraldehyde, achieving a WVP of 1.38 ± 0.04 × 10^{-9} g m^{-1} s^{-1} Pa^{-1}, an order of magnitude higher than the WVP values of the F1 and F3–F7 films.[91] Similar WVP values (1.75 ± 0.04 × 10^{-10} g m^{-1} s^{-1} Pa^{-1}) have been reported by Mu and coworkers for dialdehyde-CMC/gelatine films,[84] although the oxidation of CMC is required.

Recently, CMC films prepared with the addition of 5 wt% citric acid (CA) as the crosslinking agent were reported to show similar WVP to the ones reported in this work (1.57 × 10^{-10} g m^{-1} s^{-1} Pa^{-1}).[94,95]

The oil resistance capacity of the CMC films was measured in terms of the oil absorption rate (OAR, %), and a similar trend was observed for the OAR as that for the WVP; the films exhibited significantly improved OAR compared with F0 (see Table 3).

DSC and TGA of the CMC films

The effect of crosslinking on a polymeric material may be characterized by thermal analyses, such as DSC and TGA,[97,98] since crosslinking leads to the formation of a compact network which generally increases the thermal stability of a material.[99] In agreement with the literature, F0 shows an endothermic peak at 79 °C (T_m), due to the residual moisture on the film,[100,101] and films F1 and F3–F7 show a similar trend (Fig. 3a).[90,102] Interestingly, in the case of the crosslinked films, this peak appears at different temperatures in the DSC diagram, as is common in the literature for crosslinking of polysaccharides.[91,102] For all films tested, both onset and mid-point temperatures T_m values decrease either when the diamine alkyl-chain length decreases or, for films prepared with the same diamine, the modification degree decreases (Fig. 3b). In particular, the peak mid-point increases up to 115 °C in the case of F1. Thus, a correlation seems to exist among the moisture evaporation detected by DSC, MC (%), and modification degree. Probably, upon heating the sample, bulk water diffusion is slower through crosslinked films due to a more compact network, and its evaporation occurs at higher temperatures. In line with this hypothesis, the MC (%) of the crosslinked films is lower than that of F0 and decreases as the crosslinking degree increases (see Table 3). The hypothesis is graphically represented in Fig. 3b, in which

Table 3 MC%, MU%, WVP and OAR data[a]

Sample	MC (%)	MU (%)	WVP (10^{-10} g m^{-1} s^{-1} Pa^{-1})	OAR (%)
F0	48.3 ± 2.6[a]	98.4 ± 3.5[a]	5.86 ± 0.50[a]	0.356 ± 0.005[a]
F1	32.0 ± 1.9[b]	69.6 ± 2.1[b]	3.11 ± 0.22[b]	0.252 ± 0.005[b]
F3	34.0 ± 1.3[b]	76.0 ± 0.9[c]	3.46 ± 0.31[b]	0.276 ± 0.006[c]
F4	32.1 ± 2.9[b]	73.9 ± 3.1[c]	2.61 ± 0.15[c]	0.279 ± 0.004[c]
F5	34.1 ± 2.1[b]	71.5 ± 1.9	2.75 ± 0.17[c]	0.377 ± 0.005[a]
F6	39.2 ± 3.6[c]	75.6 ± 2.7[c]	2.63 ± 0.24[c]	0.074 ± 0.005[d]
F7	38.5 ± 4.3[c]	80.0 ± 1.5[c]	2.67 ± 0.21[c]	0.228 ± 0.004[e]

[a] Values given are mean ± standard deviation. Values with different superscripts in the same column are significantly different ($p < 0.05$).

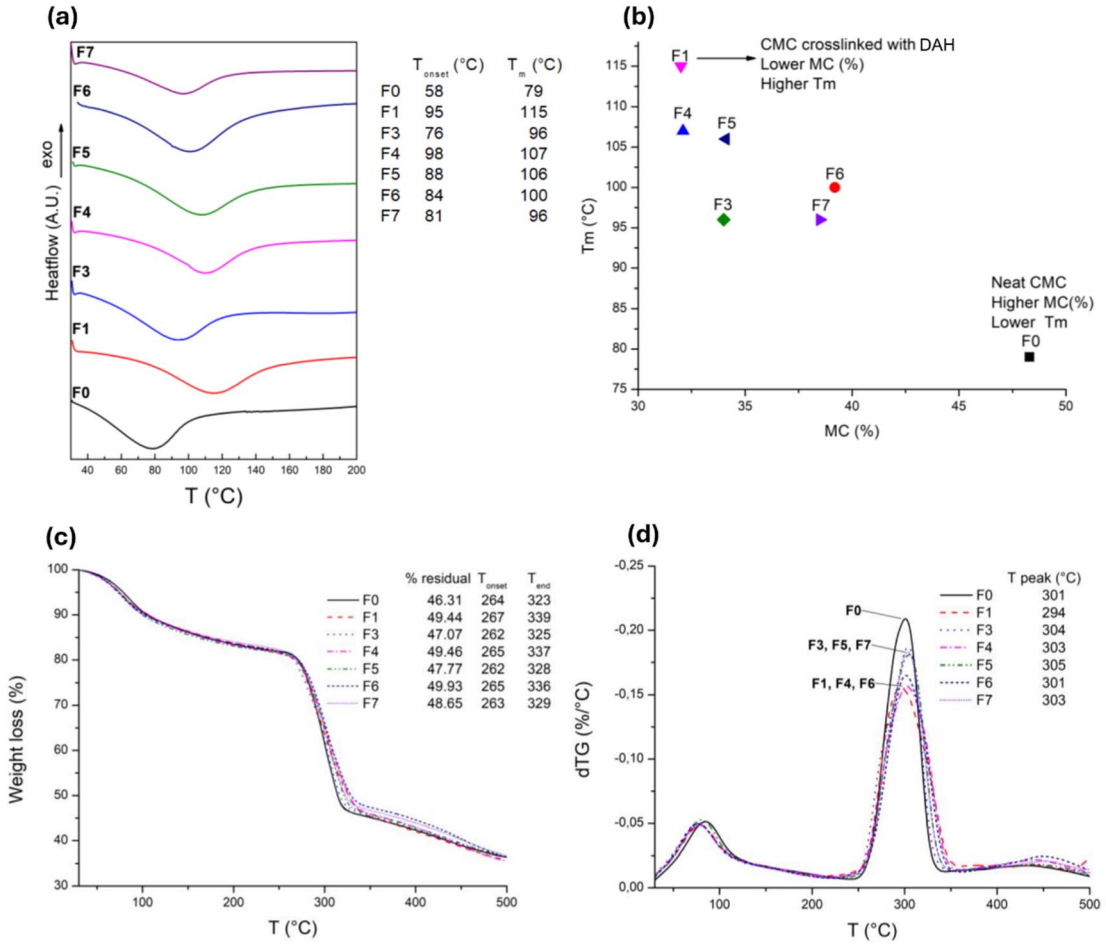

Fig. 3 (a) DSC, (b) T_m as function of MC, (c) TGA and (d) DTG of samples F0, F1, and F3–F7.

a correlation has been found between the MC (%) and the DSC moisture evaporation peak. This interesting phenomenon will be further evaluated through detailed DSC studies performed at low temperatures to detect the state of the bulk water in the crosslinked films. The graphs in Fig. 3c and d depict the TGA and TGA derivatives of F0, F1, and F3–F7, showing that all samples undergo two weight losses. The first, registered at temperatures below 100 °C, is associated with the evaporation of the residual moisture contained in the material,[101] while the second, between 240 °C and 350 °C, is the most significant and is associated with the degradation of the polymeric chains.[103,104]

The onset temperature of the starting material F0 and the crosslinked samples are listed in Fig. 3c. In particular, crosslinked samples F1, F4, and F7 showed a slightly higher onset temperature (267 °C for F1, 265 °C for F4, and 265 °C for F7) compared to the starting material F0 (264 °C) and to the films prepared with the same diamine but having lower modification degrees (262 °C for F3, 262 °C for F5, 263 °C for F7). However, significant differences were observed in the end temperature T_{end} of the thermal degradation. In fact, in this case, the crosslinked samples with high modification degrees showed significantly higher T_{end} values (339 °C for F1, 337 °C for F4, and 336 °C for F6) compared to F0 (323 °C) and to the samples having lower modification degrees (325 °C for F3, 328 °C for F5, and 329 °C for F7). This phenomenon could be associated with the slower thermal degradation of the films due to the chemical crosslinking, which retards the thermal reactions associated with CMC degradation.[105–107]

Further information can be obtained from the derivatives of the TGA (Fig. 3d), in which the degradation rate may be evaluated by the slope of the curve between 240 °C (the temperature at which degradation begins) and 350 °C (when degradation ends).[106]

As for the DSC data, TGA and dTG also evidence a significant improvement in the stabilization of films F1 and F3–F7 compared to the control sample F0 and to films prepared without the addition of a diamine (CMC/DMTMM), which degrade at temperatures between 190 °C and 300 °C.[51]

SEM analyses further confirm the presence of a highly crosslinked polymer matrix (see Fig. S26 and S27, SI).

Mechanical properties

The mechanical properties, such as the tensile strength (TS, MPa) and elongation at break (EB, %), of the crosslinked films are useful for the evaluation of their potential applications. The TS values of films F1 and F3–F5 are rather similar (Fig. 4a), while higher values were measured for films prepared with EDA,

and the TS of F6 is about 40% higher compared to that of F0 (see Fig. 4a). Considering previous TS data reported in the literature on CMC/DMTMM films and on CMC crosslinked films in the presence of citric acid,[51,95] the crosslinking degree generally plays a major role in achieving optimal TS values. On the contrary, the TS values of CMCA are not significantly affected by the amount of DMTMM used or the modification degree, as can be seen from the data plotted in Fig. 4a, while changing the diamine significantly influences TS. It is worth noting that EDA, having the shortest alkyl chain, promotes stronger contact between the polymeric chains of CMC, favourably affecting the TS.[108] In general, the improvement in the tensile strength (TS) due to crosslinking is evident, confirming the positive effect of the reaction on the mechanical performance of the films. However, when comparing the TS values with those reported in the literature (Table 4), caution is needed. Indeed, the molecular weight and degree of substitution (DS) of CMC, as well as the testing methods applied, often vary or are not explicitly reported. Moreover, in many studies, CMC is blended with other biopolymers (*e.g.*, gelatin, starch, alginate, chitosan), which can significantly affect its mechanical properties and hinder direct comparison.

A more consistent benchmark can be found in our previous work,[51] where CMC was crosslinked with DMTMM in the

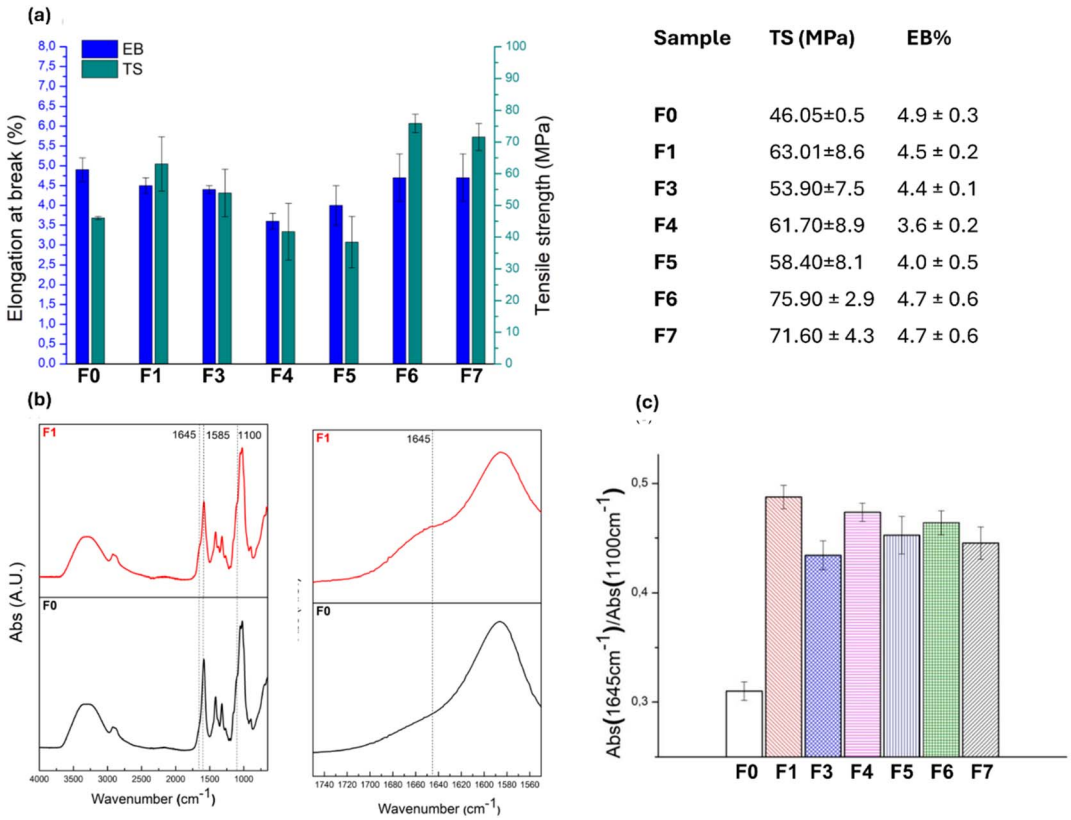

Fig. 4 (a) TS, EB of samples F0, F1, and F3–F7, (b) ATR-FTIR spectra of F1 (red line) and F0 (black line) films, and (c) Abs (1645 cm^{-1})/Abs (1100 cm^{-1}) ratios for samples F0, F1, and F3–F7.

Table 4 Comparison of the TS values of the CMC-based films reported in the literature

TS (MPa)	Material	MW_{CMC} (Da)	DS_{CMC}	Testing method	Ref.
29.6 ± 3.0	CMC + H_2SO_4	90 000	0.7	—[e]	Wang *et al.*, 2021 (ref. 33)
54.9 ± 3.1	CMC crosslinked with DMTMM	90 000	0.7	ASTM D882-91	Beghetto *et al.*, 2020 (ref. 51)
22.9 ± 0.9	CMC + $CaCl_2$ + gelatine	—[a]	—	ASTM D882-12	He *et al.*, 2022 (ref. 109)
78.2 ± 11.7	CMC + SA + CS[b]	—	—	—[f]	Lan *et al.*, 2018 (ref. 110)
32.6 ± 2.1	CMC + starch	—	—	ASTM D882-12	Tavares *et al.*, 2020 (ref. 104)
30.0 ± 2.0	CMC[c] + starch	150 000	—	ASTM D882-12	Tongdeesoontorn *et al.*, 2020 (ref. 111)
15.1 ± 1.2	DCMC[d] + gelatine	—	—	ASTM D882-97	Mu *et al.*, 2012 (ref. 84)
75.9 ± 2.9	CMC crosslinked with EDA	90 000	0.7	ASTM D882-91	F6 (this work)

[a] CMC (%) viscosity at 25 °C: 800–1200 mPa s. [b] SA: sodium alginate; CS: chitosan. [c] AKUCELL-AF 0705. [d] DCMC: dialdehyde CMC. [e] 5 mm wide and 30 mm long strip; the gauge of the strips was 20 mm and the strain rate was 25 mm min^{-1}. [f] 80 mm × 150 mm; return distance of 60 mm, speed of 5 mm s^{-1}, effective elongation distance of 80 mm, and trigger force of 5 N.

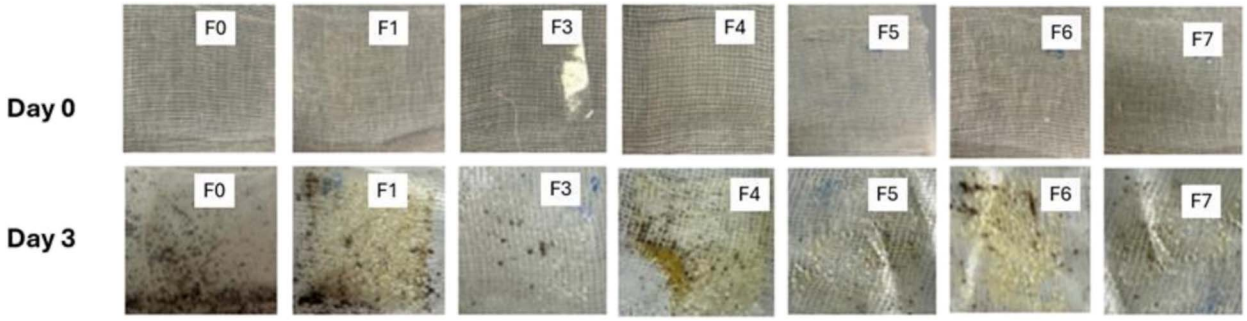

Fig. 5 Day 0 and day 3 pictures of the F0–F6 films during the biofragmentation process.

absence of diamines, resulting in a TS of 54.9 ± 3.1 MPa. The higher TS values obtained in the present work, therefore, indicate that the introduction of the diamine has a beneficial effect, further enhancing the mechanical strength of the films. This improvement may be rationalized by considering that diamines can promote a more efficient linkage between different polymer chains, leading to a denser and more interconnected network. In addition, the presence of aliphatic chains in the diamine may contribute to a more favorable packing of the material, ultimately reinforcing the overall tensile strength.

ATR-FTIR analysis

ATR-FTIR analysis of all films has been performed (see Fig. S22 in SI), and only F0 and F1 are reported as representative in Fig. 4b. Comparing F0 to F1, a band at 1645 cm^{-1} in the ATR-FTIR spectrum of F1 confirms the formation of amide bonds promoted by DMTMM, in agreement with the literature,[66,112,113] and no other relevant differences are present in the ATR-FTIR spectra of F0 and F1. A semi-quantitative estimation of the amount of amide bonds formed was obtained by dividing the absorbance at 1645 cm^{-1} (Abs 1645) by the absorbance at 1100 cm^{-1} (Abs 1100) of the AGU unit, which is not affected by the crosslinking reaction (see Fig. 4c).[106,112,114]

From this data a significant variation ($p < 0.05$) in the Abs 1645/1100 ratio is observed on comparing F0 to F1 and F3–F7, confirming that a higher crosslinking degree of the polymer matrix is obtained with 30 wt% DMTMM by weight of CMC.

Visual biofragmentation of films

Biofragmentation is a crucial step in the biodegradation process, where catalytic agents (*e.g.* enzymes) produced by microorganisms gradually break up polymeric chains into smaller molecules,[115,116] followed by assimilation and mineralization stages. The biofragmentation of films F0, F1, and F3–F7 was performed according to the literature, with slight modifications[66,72] involving burying the films under 2 cm of soil and spraying the soil with water once a day. Pictures of all samples at day 0 and after three days of burial are shown in Fig. 5.

From the visual analysis (Fig. 5), it was possible to observe that after three days, all samples were highly fragmented, and only a modest difference in colour between F1, F4, and F6 and F3, F5 and F7 was evidenced. Although it was not possible to weigh films F0, F1, and F3–F7 due to soil contamination and the advanced degradation state of the films at day 3, all samples were completely biofragmented after seven days, demonstrating comparable biofragmentation between the films tested and the control sample. It should be noted that this test represents a qualitative assessment, mainly aiming to verifying that the crosslinking process does not significantly compromise the intrinsic biodegradability of CMC.

Conclusions

This paper reports the first example of amidated crosslinked CMC films (CMCA) prepared by a reaction between CMC and an aliphatic diamine (ethylenediamine, butyldiamine, hexamethylenediamine), promoted by DMTMM. The influence of the length of the diamine alkyl chain and the COONa/diamine/DMTMM molar ratio on the properties of the CMCA films was investigated. The structure of the newly prepared CMCA was confirmed by mono and bidimensional NMR studies. Interestingly, ^{1}H NMR and HMBC studies provided clear-cut information on the nature of the bonds contributing to the CMCA crosslinking. In particular, the formation of stable covalent bonds was demonstrated, excluding the presence of ionic interactions and highlighting the key role of DMTMM in the formation of the crosslinking. Overall, the efficiency of DMTMM was between 30% and 41%, and the highest MoD_{NMR} of 9.75 was measured for the EDA-crosslinked CMC films. Statistical analysis of the physical–mechanical data clearly evidenced that the characteristics of the films are mainly influenced by the diamine alkyl chain length. The positive effect of diamine addition on the barrier and water vapour absorption properties can be rationalized by the presence of the hydrophobic alkyl chains and the highly efficient packing of the CMC chains induced by crosslinking, which inhibit and retard water uptake and its subsequent diffusion within the film matrix.

Similarly, the diamines also play a key role in enhancing the mechanical properties. This is probably due to the hydrophobic interactions established between the diamine chains, which provide an additional contribution to the structural integrity of the material and consequently improve its tensile strength.

The best water vapour permeability ($2.63 \pm 0.24 \times 10^{-10}$ g m^{-1} s^{-1} Pa^{-1}), oil resistance ($7.4 \pm 0.5 \times 10^{-2}$%), and one of the highest tensile strength value ever reported for CMC films (TS

75.90 ± 2.90 MPa) were obtained with a COONa/EDA/DMTMM molar ratio of 6/1/2 (F6, Table 1). DSC, TGA, SEM and ATR-FTIR analysis further confirmed the formation of strong covalent bonds between CMC and the diamines, promoted by DMTMM. All the prepared films showed high transparency values, with the best film F6 exhibiting an exceptionally high barrier to UVC, a valuable characteristic for food preservation. Overall, the data demonstrate that CMCA is a highly performing biodegradable film, prepared with an easy, safe, and promising approach suitable for food packaging applications. Studies are ongoing to test the shelf life of food samples packaged in CMCA films to further validate their applicability. It should be noted that the primary goal of this work was to provide a proof of concept, demonstrating the direct correlation between diamine cross-linking and improvement of functional properties. Critical aspects, such as long-term safety and biocompatibility, as well as the scalability of the preparation process, remain to be further investigated. Moreover, biofragmentation was assessed only through visual inspection, representing a qualitative rather than quantitative evaluation. Therefore, future studies using respirometric methods and quantitative CO_2 release measurements should be conducted on these amidated cellulosic derivatives.

Author contributions

Domenico Santandrea: conceptualization, investigation, validation, data curation, formal analysis, writing – original draft; Valentina Beghetto: conceptualization, validation, formal analysis, writing – review & editing, fundraising.

Conflicts of interest

There are no conflicts to declare.

Data availability

All data supporting the findings of this study are available within the article and its SI files. Supplementary information: ^{1}H and ^{13}C NMR spectra (including COSY, HSQC, and HMBC), ATR-FTIR spectra, MU%, WVP, and OAR% data, SEM images, product yields, and elemental analysis calculations. See DOI: **https://doi.org/10.1039/d5ra05273d**.

Acknowledgements

The research described in this article was made possible by funding from the Food-4-Life project, co-funded by the European Union under the PR Veneto FESR 2021–2027 program, Action 1.1.1. The Unique Project Code (CUP) is D19J24000670007 and the Fund CUP code is H19C23000170009. The work was supported by the PNRR funding for the 38th PhD cycle "Dottorato d'interesse Nazionale in Desing per il Made in Italy: Identità, Innovazione e Sostenibilità", administrative headquarter University Vanvitelli, Caserta (Italy). The authors wish to thank Prof. J. Bras and his staff from the Grenoble INP-Pagora, UGA, for the support in physical–mechanical characterisation of the samples, Prof. D. Battistel (Ca' Foscari University of Venice) for the support in statistical analysis, A. Campostrini (Ca' Foscari University of Venice) for the support in colorimetric analysis, and Prof. M. Bortoluzzi (Ca' Foscari University of Venice), S. Conca and N. Bardella (Crossing srl) for the support in NMR characterization.

References

1 D. Luo, X. Chu, Y. Wu, Z. Wang, Z. Liao, X. Ji, J. Ju, B. Yang, Z. Chen, R. Dahlgren, M. Zhang and X. Shang, *J. Hazard. Mater.*, 2024, **465**, 133412.
2 R. C. Hale, M. E. Seeley, M. J. La Guardia, L. Mai and E. Y. Zeng, *J. Geophys. Res.: Oceans*, 2020, **125**(1), e2018JC014719.
3 C. M. C. Richard, E. Dejoie, C. Wiegand, G. Gouesbet, H. Colinet, P. Balzani, D. Siaussat and D. Renault, *J. Hazard. Mater.*, 2024, **477**, 135299.
4 J. R. Jambeck, R. Geyer, C. Wilcox, T. R. Siegler, M. Perryman, A. Andrady, R. Narayan and K. L. Law, *Science*, 2015, **347**, 768–771.
5 A. D. Vethaak and J. Legler, *Science*, 2021, **371**, 672–674.
6 P. Choudhary, A. Pathak, P. Kumar, C. S and N. Sharma, *Biomass Convers. Biorefin.*, 2024, **14**, 10817–10827.
7 J. Cheng, R. Gao, Y. Zhu and Q. Lin, *Alex. Eng. J.*, 2024, **91**, 70–83.
8 M. J. Getahun, B. B. Kassie and T. S. Alemu, *Process Biochem.*, 2024, **145**, 261–287.
9 A. Jha and A. Kumar, *Bioprocess Biosyst. Eng.*, 2019, **42**, 1893–1901.
10 B. Dey, M. R. Prabhakar, S. Jayaraman, L. K. S. Gujjala, A. P. Venugopal and P. Balasubramanian, *Food Res. Int.*, 2024, **191**, 114723.
11 S. N. Fatima, *Mater. Today Commun.*, 2024, **40**, 109846.
12 S. Sayanjali, Y. Lu and K. Howell, *Int. J. Food Sci.*, 2024, **2024**, 1–15.
13 E. Kabir, R. Kaur, J. Lee, K.-H. Kim and E. E. Kwon, *J. Clean. Prod.*, 2020, **258**, 120536.
14 European Bioplastics e.V., **https://www.european-bioplastics.org/**, accessed July 21, 2025.
15 M. Lalanne-Tisné, S. Eyley, J. De Winter, A. Favrelle-Huret, W. Thielemans and P. Zinck, *Carbohydr. Polym.*, 2022, **295**, 119840.
16 S. R. Kanatt and S. H. Makwana, *Carbohydr. Polym.*, 2020, **227**, 115303.
17 G. E. Luckachan and C. K. S. Pillai, *J. Polym. Environ.*, 2011, **19**, 637–676.
18 D. Klemm, B. Heublein, H. Fink and A. Bohn, *Angew. Chem., Int. Ed.*, 2005, **44**, 3358–3393.
19 L. Duchatel-Crépy, N. Joly, P. Martin, A. Marin, J.-F. Tahon, J.-M. Lefebvre and V. Gaucher, *Carbohydr. Polym.*, 2020, **234**, 115912.
20 R. R. Kurhade, M. S. Shaikh, V. Nagulwar and M. A. Kale, *Int. J. Polym. Mater. Polym. Biomater.*, 2025, **74**, 1043–1067.
21 A. M. Omer, W. A.-A. Sadik, R. A. Elady, T. M. Tamer, M. M. Abd-Ellatif and M. S. Mohy-Eldin, *Desalination Water Treat.*, 2024, **317**, 100041.

22 B. B. Kassie, T. M. Daget and D. F. Tassew, *Int. J. Biol. Macromol.*, 2024, **278**, 134990.
23 E. M. Elnaggar, M. S. Abusaif, Y. M. Abdel-Baky, A. Ragab, A. M. Omer, I. Ibrahim and Y. A. Ammar, *Int. J. Biol. Macromol.*, 2024, **277**, 134347.
24 N. Jabeen and M. Atif, *Polym. Adv. Technol.*, 2024, **35**(1), e6203.
25 I. Šimkovic, F. Gucmann, M. Hricovíni, R. Mendichi, A. G. Schieroni, D. Piovani, S. Zappia, E. Dobročka, J. Filip and M. Hricovíni, *Cellulose*, 2023, **30**, 2023–2036.
26 R. Ramakrishnan, J. T. Kim, S. Roy and A. Jayakumar, *Int. J. Biol. Macromol.*, 2024, **259**, 129194.
27 M. Yildirim-Yalcin, F. Tornuk and O. S. Toker, *Trends Food Sci. Technol.*, 2022, **129**, 179–193.
28 E. Pinto, W. N. Aggrey, P. Boakye, G. Amenuvor, Y. A. Sokama-Neuyam, M. K. Fokuo, H. Karimaie, K. Sarkodie, C. D. Adenutsi, S. Erzuah and M. A. D. Rockson, *Sci. Afr.*, 2022, **15**, e01078.
29 Y. Xu, Q. Deng, C. Ruan, D. Xu and K. Zeng, *Packag. Technol. Sci.*, 2024, **37**, 781–792.
30 R. Sole, L. Taddei, C. Franceschi and V. Beghetto, *Molecules*, 2019, **24**, 2979.
31 T. P. Haider, C. Völker, J. Kramm, K. Landfester and F. R. Wurm, *Angew. Chem., Int. Ed.*, 2019, **58**, 50–62.
32 M. Alfindee, Z. Sweah and T. Saki, *Egypt. J. Chem.*, 2021, **64**(5), 2679–2684.
33 M. Wang, X. Jia, W. Liu and X. Lin, *Carbohydr. Polym.*, 2021, **255**, 117353.
34 F. S. Alatawi, M. Monier and N. H. Elsayed, *Int. J. Biol. Macromol.*, 2018, **114**, 1018–1025.
35 D. Charpentier, G. Mocanu, A. Carpov, S. Chapelle, L. Merle and G. Müller, *Carbohydr. Polym.*, 1997, **33**, 177–186.
36 N. M. Zabivalova, A. M. Bochek, L. M. Kalyuzhnaya, E. N. Vlasova and B. Z. Volchek, *Russ. J. Appl. Chem.*, 2003, **76**, 1998–2002.
37 T. Taubner, A. Synytsya and J. Čopíková, *Int. J. Biol. Macromol.*, 2015, **72**, 11–18.
38 A. Pettignano, A. Charlot and E. Fleury, *Polym. Rev.*, 2019, **59**, 510–560.
39 S. Dacrory, H. Abou-Yousef, S. Kamel, R. E. Abou-Zeid, M. S. Abdel-Aziz and M. Elbadry, *Cellul. Chem. Technol.*, 2019, **53**, 23–33.
40 S. Grabska-Zielińska, *Polymers*, 2024, **16**, 2679.
41 F. Ren, H. Ding, B. Dong, X. Qian, J. Liu and J. Tan, *Constr. Build. Mater.*, 2024, **415**, 135101.
42 C. N. Munyiri, E. S. Madivoli, J. Kisato, J. Gichuki and P. G. Kareru, *Int. J. Polym. Mater. Polym. Biomater.*, 2025, **74**, 625–640.
43 A. C. Alavarse, E. C. G. Frachini, R. L. C. G. Da Silva, V. H. Lima, A. Shavandi and D. F. S. Petri, *Int. J. Biol. Macromol.*, 2022, **202**, 558–596.
44 S. Paganelli, N. Massimi, A. Di Michele, O. Piccolo, R. Rampazzo, M. Facchin and V. Beghetto, *Int. J. Biol. Macromol.*, 2024, **270**, 132541.
45 H. Nasution, H. Harahap, N. F. Dalimunthe, M. H. S. Ginting, M. Jaafar, O. O. H. Tan, H. K. Aruan and A. L. Herfananda, *Gels*, 2022, **8**, 568.
46 X. Hou, L. Lin, K. Li, F. Jiang, D. Qiao, B. Zhang and F. Xie, *Adv. Colloid Interface Sci.*, 2024, **325**, 103113.
47 G. Tillet, B. Boutevin and B. Ameduri, *Prog. Polym. Sci.*, 2011, **36**, 191–217.
48 J. Pan, Y. Li, K. Chen, Y. Zhang and H. Zhang, *Carbohydr. Polym.*, 2021, **266**, 118102.
49 T. Yang, C. Xu, C. Liu, Y. Ye, Z. Sun, B. Wang and Z. Luo, *Chem. Eng. J.*, 2022, **429**, 132430.
50 G. Leone, M. Delfini, M. E. Di Cocco, A. Borioni and R. Barbucci, *Carbohydr. Res.*, 2008, **343**, 317–327.
51 V. Beghetto, V. Gatto, S. Conca, N. Bardella, C. Buranello, G. Gasparetto and R. Sole, *Carbohydr. Polym.*, 2020, **249**, 116810.
52 R. Sole, C. Buranello, A. Di Michele and V. Beghetto, *Int. J. Biol. Macromol.*, 2022, **209**, 2009–2019.
53 Q. Mo, L. Huang, Y. Sheng, Z. Wei, S. Zhang, Y. Li, X. Wang, Y. Wang, X. Lu, C. Huang, Q. Duan and M. Xue, *Food Hydrocolloids*, 2024, **154**, 110079.
54 M. Zhang, W. Choi, M. Kim, J. Choi, X. Zang, Y. Ren, H. Chen, V. Tsukruk, J. Peng, Y. Liu, D. H. Kim and Z. Lin, *Angew. Chem., Int. Ed.*, 2024, **136**(24), e202318035.
55 R. Sole, L. Agostinis, V. Beghetto, S. Conca, V. Gatto, N. Bardella, A. Morandini and C. Buranello, *Synthesis*, 2021, **53**, 1672–1682.
56 N. A. Dahlan, S. Y. Teow, Y. Y. Lim and J. Pushpamalar, *Express Polym. Lett.*, 2021, **15**, 612–625.
57 M. D'Este, D. Eglin and M. Alini, *Carbohydr. Polym.*, 2014, **108**, 239–246.
58 M. Kunishima, C. Kawachi, J. Monta, K. Terao, F. Iwasaki and S. Tani, *Tetrahedron*, 1999, **55**, 13159–13170.
59 R. Sole, V. Gatto, S. Conca, N. Bardella, A. Morandini and V. Beghetto, *Molecules*, 2021, **26**, 191.
60 A. Morandini, B. Leonetti, P. Riello, R. Sole, V. Gatto, I. Caligiuri, F. Rizzolio and V. Beghetto, *ChemMedChem*, 2021, **16**, 3172–3176.
61 Z. Wang, T. Huang, Z. Liu and A. Yu, *Electrochim. Acta*, 2021, **389**, 138806.
62 V. Beghetto, L. Agostinis, V. Gatto, R. Samiolo and A. Scrivanti, *J. Clean. Prod.*, 2019, **220**, 864–872.
63 Z. Zhai, Y. Zhou, A. G. Korovich, B. A. Hall, H. Y. Yoon, Y. Yao, J. Zhang, M. J. Bortner, M. Roman, L. A. Madsen and K. J. Edgar, *Biomacromolecules*, 2023, **24**, 2596–2605.
64 V. Beghetto, V. Gatto, S. Conca, N. Bardella and A. Scrivanti, *Molecules*, 2019, **24**, 3611.
65 V. Gatto, S. Conca, N. Bardella and V. Beghetto, *Materials*, 2021, **14**, 3069.
66 D. Santandrea, C. Sillard, V. Beghetto and J. Bras, *ChemPlusChem*, 2025, 202500398.
67 A. Kumar, B. Watbled, I. Baussanne, S. Hediger, M. Demeunynck and G. De Paëpe, *Commun. Chem.*, 2023, **6**, 58.
68 Q. Lin, J. Chang, M. Gao and H. Ma, *J. Environ. Sci. Health, Part A: Toxic/Hazard. Subst. Environ. Eng.*, 2017, **52**, 106–116.
69 P. D. Dalton, C. Hostert, K. Albrecht, M. Moeller and J. Groll, *Macromol. Biosci.*, 2008, **8**, 923–931.

70 C. Demitri, R. Del Sole, F. Scalera, A. Sannino, G. Vasapollo, A. Maffezzoli, L. Ambrosio and L. Nicolais, *J. Appl. Polym. Sci.*, 2008, **110**, 2453–2460.
71 A. Sannino, C. Demitri and M. Madaghiele, *Materials*, 2009, **2**, 353–373.
72 D. Piñeros-Hernandez, C. Medina-Jaramillo, A. López-Córdoba and S. Goyanes, *Food Hydrocolloids*, 2017, **63**, 488–495.
73 T. Borke, F. M. Winnik, H. Tenhu and S. Hietala, *Carbohydr. Polym.*, 2015, **116**, 42–50.
74 A. Heydari, N. Borazjani, F. Kazemi-Aghdam, J. Filo and I. Lacík, *Carbohydr. Polym.*, 2025, **348**, 122893.
75 H. Kono, *Carbohydr. Polym.*, 2014, **106**, 84–93.
76 F. Yu, H. Shi, K. Wang, H. Li and L. Peng, *Int. J. Biol. Macromol.*, 2022, **222**, 1238–1249.
77 F. F. L. Ho and D. W. Klosiewicz, *Anal. Chem.*, 1980, **52**, 913–916.
78 T. Heinze and K. Pfeiffer, *Angew. Makromol. Chem.*, 1999, **266**, 37–45.
79 H. Kono, K. Oshima, H. Hashimoto, Y. Shimizu and K. Tajima, *Carbohydr. Polym.*, 2016, **146**, 1–9.
80 D. Ruhr, M. John and A. Reiche, *Carbohydr. Polym.*, 2021, **251**, 117043.
81 K. Thompson and S. Michielsen, *J. Polym. Sci., Part A: Polym. Chem.*, 2006, **44**, 126–136.
82 E. J. Cozens, N. Roohpour and J. E. Gautrot, *Eur. Polym. J.*, 2021, **146**, 110250.
83 O. L. Vidal, A. Tsukui, R. Garrett, M. H. M. Rocha-Leão, C. W. P. Carvalho, S. P. Freitas, C. M. De Rezende and M. S. L. Ferreira, *Int. J. Biol. Macromol.*, 2020, **146**, 730–738.
84 C. Mu, J. Guo, X. Li, W. Lin and D. Li, *Food Hydrocolloids*, 2012, **27**, 22–29.
85 A. C. M. De Moraes, P. F. Andrade, A. F. De Faria, M. B. Simões, F. C. C. S. Salomão, E. B. Barros, M. D. C. Gonçalves and O. L. Alves, *Carbohydr. Polym.*, 2015, **123**, 217–227.
86 X.-F. Zhang, L. Song, Z. Wang, Y. Wang, L. Wan and J. Yao, *Int. J. Biol. Macromol.*, 2020, **145**, 663–667.
87 N. Shuzhen, J. Liang, Z. Hui, Z. Yongchao, F. Guigan, X. Huining and D. Hongqi, *R. Soc. Open Sci.*, 2018, **5**, 181206.
88 I. Leceta, P. Guerrero and K. De La Caba, *Carbohydr. Polym.*, 2013, **93**, 339–346.
89 H. Li, X. Gao, Y. Wang, X. Zhang and Z. Tong, *Int. J. Biol. Macromol.*, 2013, **52**, 275–279.
90 A. E. Gasperini, S. Sanchez, A. L. Doiron, M. Lyles and G. K. German, *Sci. Rep.*, 2017, **7**(1), 6631.
91 M. Shahbazi, S. J. Ahmadi, A. Seif and G. Rajabzadeh, *Food Hydrocolloids*, 2016, **61**, 378–389.
92 B. Ghanbarzadeh, H. Almasi and A. A. Entezami, *Innov. Food Sci. Emerg. Technol.*, 2010, **11**, 697–702.
93 Z. J. Kamiński, *Biopolymers*, 2000, **55**, 140–164.
94 T. Nongnual, N. Butprom, S. Boonsang and S. Kaewpirom, *Int. J. Biol. Macromol.*, 2024, **267**, 131135.
95 T. J. Hickman, L. Tao, N. Stingelin and J. C. Meredith, *RSC Sustain.*, 2024, **2**, 3451–3455.
96 S. Mukherjee, A. Sengupta, S. Preetam, T. Das, T. Bhattacharya and N. Thorat, *Carbohydr. Polym. Technol. Appl.*, 2024, **7**, 100505.
97 A. Riaz, C. Lagnika, H. Luo, M. Nie, Z. Dai, C. Liu, M. Abdin, M. M. Hashim, D. Li and J. Song, *Carbohydr. Polym.*, 2020, **235**, 115944.
98 W. C. Chen, S. N. M. S. Mohd Judah, S. K. Ghazali, D. I. Munthoub, H. Alias, Z. Mohamad and R. A. Majid, *Chem. Eng. Trans.*, 2021, **83**, 199–204.
99 C. G. T. Neto, J. A. Giacometti, A. E. Job, F. C. Ferreira, J. L. C. Fonseca and M. R. Pereira, *Carbohydr. Polym.*, 2005, **62**, 97–103.
100 S. El-Sayed, K. H. Mahmoud, A. A. Fatah and A. Hassen, *Phys. B*, 2011, **406**, 4068–4076.
101 S. Roy and J.-W. Rhim, *Int. J. Biol. Macromol.*, 2020, **148**, 666–676.
102 G. Priya, U. Narendrakumar and I. Manjubala, *J. Therm. Anal. Calorim.*, 2019, **138**, 89–95.
103 H. M. S. Akhtar, A. Riaz, Y. S. Hamed, M. Abdin, G. Chen, P. Wan and X. Zeng, *Int. J. Biol. Macromol.*, 2018, **118**, 469–477.
104 K. M. Tavares, A. D. Campos, B. R. Luchesi, A. A. Resende, J. E. D. Oliveira and J. M. Marconcini, *Carbohydr. Polym.*, 2020, **246**, 116521.
105 I. Šimkovic, A. Tracz, I. Kelnar, I. Uhliariková and R. Mendichi, *Carbohydr. Polym.*, 2014, **99**, 356–364.
106 G. Stiubianu, A. Nicolescu, A. Nistor, M. Cazacu, C. Varganici and B. C. Simionescu, *Polym. Int.*, 2012, **61**, 1115–1126.
107 F. Jiang and Y.-L. Hsieh, *ACS Appl. Mater. Interfaces*, 2017, **9**, 2825–2834.
108 A. Strand, A. Sundberg, E. Retulainen, K. Salminen, A. Oksanen, J. Kouko, A. Ketola, A. Khakalo and O. Rojas, *Nord. Pulp Pap. Res. J.*, 2017, **32**, 324–335.
109 B. He, S. Wang, P. Lan, W. Wang and J. Zhu, *Food Chem.*, 2022, **382**, 132391.
110 W. Lan, L. He and Y. Liu, *Coatings*, 2018, **8**, 291.
111 W. Tongdeesoontorn, L. J. Mauer, S. Wongruong, P. Sriburi and P. Rachtanapun, *Polymers*, 2020, **12**, 366.
112 M. Le Gars, A. Delvart, P. Roger, M. N. Belgacem and J. Bras, *Colloid Polym. Sci.*, 2020, **298**, 603–617.
113 A. Bendahou, A. Hajlane, A. Dufresne, S. Boufi and H. Kaddami, *Res. Chem. Intermed.*, 2015, **41**, 4293–4310.
114 S. Cichosz and A. Masek, *Materials*, 2020, **13**, 4573.
115 R. R. A. Silva, C. S. Marques, T. R. Arruda, S. C. Teixeira and T. V. De Oliveira, *Macromol*, 2023, **3**, 371–399.
116 O. K. Cakmak, *Circ. Econ. Sustainability*, 2024, **4**, 339–362.